APPLIED SCIENCES AND ENGINEERING

Soft sensors for a sensing-actuation system with high bladder voiding efficiency

F. Arab Hassani[1,2]*, H. Jin[2], T. Yokota[2], T. Someya[2,3,4], N. V. Thakor[1,3,5]*

Sensing-actuation systems can assist a bladder with lost sensation and weak muscle control. Here, we advance the relevant technology by integrating a soft and thin capacitive sensor with a shape memory alloy–based actuator to achieve a high-performance closed-loop configuration. In our design, sensors capable of continuous bladder volume detection and actuators with strong emptying force have been used. This integration has previously hindered performance due to large bladder volume changes. Our solution integrates sensing-actuation elements that are bladder compatible but do not interfere with one another, achieving real-time bladder management. The system attains a highly desirable voiding target of 71 to 100% of a rat's bladder with a volume sensitivity of 0.7 μF/liter. Our system represents an efficient voiding solution that avoids overfilling and represents a technological solution to bladder impairment treatment, serving as a model for similar soft sensor-actuator integration with other organs.

INTRODUCTION

The development of artificial organs that can mimic the complex and delicate human vital organs has the potential for taking us closer to eliminating the need for transplantation (*1*). Soft electronics technology can be of particular value for interfacing with soft and compliant organs like brain, nerves, heart, and bladder (*2*, *3*). Soft sensors attached to these organs can retrieve the organ's functional signature, while soft actuators can empower these artificial organs to reinstate the lost function of the failed organs (*4*, *5*). In particular, the combination of soft sensors and actuators can provide a soft system solution for on-time organ assistance (*6*, *7*). The soft systems not only have substantial mechanical compliance with living tissue, but they are also capable of performing complex tasks over rigid systems (*8*, *9*). For example, the urinary bladder is unique among organs as it undergoes large volume changes during the storage and urination phases (*3*). The human bladder can expand up to five times its empty state volume for the storage of about 500 ml of urine (*10*). Therefore, development of an assistance solution for a dysfunctional bladder requires careful compatibility considerations to avoid interference with these extreme volume changes. Neurogenic underactive bladder (UAB) is a condition that may arise following a spinal cord injury (SCI) (*11*). SCI prevalence is reported at 236 to 1009 per 1,000,000 people (*12*), and about 80% of patients with SCI suffer from some degree of bladder dysfunction (*13*). Patients with neurogenic UAB may endure dysfunction from loss of bladder sensation and a weak bladder muscle (*11*). As a result, an assistive solution that senses bladder volume during storage and actuates for urination is required for these patients. Besides a wide dynamic range for stretch sensing, the sensor must be soft and compliant as well. The bladder system actuator must also facilitate complete bladder emptying to circumvent a postvoid residual volume (*14*). Such a soft system can also be adopted for assisting other organs with peristaltic movements, such as blood vessels, esophagus, stomach, and intestines (*15*, *16*).

Recent advances in soft materials and their fabrication techniques allow the development of sensors and actuators compatible with soft organs (*17*). This technology has been most evident in the application of thin and flexible sensing electrodes for physiological signals monitoring from skin (*18*), heart (*7*), and brain surfaces (*19*). The additional stretchable property of these materials makes them suitable for tactile strain sensing applications (*9*, *20*, *21*). The direct integration of these strain sensors with the bladder for volume detection requires materials with a lower modulus than the bladder muscle (*3*, *22*–*27*). This property allows normal expansion and shrinkage of the bladder for muscle distention measurement during the storage (*23*). Because of large bladder volume changes, the interface between these strain sensors and the bladder was maintained via suturing (*22*, *24*), adhesives (*3*), or circumferential bladder wrapping (*23*, *25*).

The electrical stimulation of nerves (*28*), muscles (*29*), heart (*7*), and brain (*6*) using flexible electrodes has been introduced for triggering soft organs with failed functionality. Alternately, several soft actuators have been reported to assist weak organs in performance recovery such as the pneumatic actuating sleeves for heart muscle assistance (*30*) and soft cuffs and shape memory alloy (SMA) artificial sphincters for fecal and urinary continence recovery (*31*). For bladder elasticity matching, soft electrical stimulation actuators have been reported to void the bladder (*22*, *23*, *32*). These actuators consist of soft electrodes that are directly attached on the bladder surface for electrical stimulation of the muscle (*22*) or its related nerves (*23*). To avoid possible electrical stimulation of untargeted neighboring muscles or nerves, soft actuators capable of physical bladder compression have been developed (*33*). These actuators were compatible with bladder volume changes and capable of voiding 25% of the bladder in one activation cycle (*33*). SMA-based actuators with bistable characteristics were able to efficiently advance, voiding up to about 80% (*34*).

Previous integration of soft sensing and stimulation electrodes on the heart or brain surface demonstrated the importance of integrated systems for real-time organ monitoring and stimulation (*7*, *19*, *35*). Analogously, integration of a bladder stretch sensor would help detect fullness status and activate the bladder compression

[1]Department of Biomedical Engineering, National University of Singapore, 28 Medical Drive, #05-COR, Singapore 117456, Singapore. [2]Department of Electrical Engineering and Information Systems, The University of Tokyo, Tokyo 113-8656, Japan. [3]Department of Electrical and Computer Engineering, Faculty of Engineering, National University of Singapore, 4 Engineering Drive 3, #05-45, Singapore 117583, Singapore. [4]Thin-Film Device Laboratory, RIKEN, Saitama 351-0198, Japan. [5]Department of Biomedical Engineering, Johns Hopkins University, 720 Rutland Avenue, Baltimore, MD 21205, USA.
*Corresponding author. Email: faezeh.arabhassani@gmail.com (F.A.H.); thakornus@gmail.com (N.V.T.)

actuator following notification. The integration of thermoresponsive actuators with strain sensors demonstrated an integrated system with the required softness for bladder interaction (*25*). In the previous design, the actuator emptied only about 15% of the urine due to its softness (*25*). Similarly, the integration of multilayered triboelectric energy harvesting (TENG) sensors with bistable SMA-based actuators achieved an integrated system capable of volume detection and urine voiding (*34*). The actuator was capable of voiding 43% of bladder volume because of the presence of thick TENG sensor (*34*).

However, a voiding efficiency of at least 80% is recommended to avoid retention of more than 100 ml of postvoid residual volume and consequent complications (*14*). Moreover, an ideal integrated system demands both volume sensing capability and high voiding efficiency; this is a challenge considering the bladder volume changes from 0 to 500 ml during storage and vice versa during urination. In other words, the bladder system needs thin and soft sensors with modulus lower than the bladder muscle for accurate volume detection and minimum interference with actuator performance. In contrast, the bladder system requires actuators that are stiffer than the bladder muscle for voiding most of the urine. The inability to achieve both conditions results in bladder overfilling during storage and only partial bladder emptying during voiding, resulting in severe medical complications (*11*).

In the current study, we show an integrated bladder system for bladder control, consisting of both soft sensors, responsive to the continuous volume change, and flexible SMA-based actuators with high voiding efficiency. We demonstrate an interdigitated capacitive sensor capable of repeatable volume detection with a sensitivity of 0.7 and 1.8 μF/liter during the urine storage and voiding phases, respectively. The high sensitivity of the sensor during both storage and voiding phases is the result of its wrinkled structure that operates similar to bladder muscle receptors with dual functionality of normal and stretching force sensation. Also, the minimum sensor interference with the actuator performance results in a high voiding efficiency between 71 and 100% for one activation cycle. Moreover, the actuator includes an SMA spring, which aids in keeping the sensor in contact with the bladder surface at all times, for precise volume detection. Therefore, unlike the stretchable strain sensors, the cumbersome direct sensor adherence onto the bladder surface can be avoided. In vitro tests demonstrate the repeatable performance of the integrated system during storage and actuation phases. Last, the integrated bladder system is implanted in three rats for in vivo characterization, and the results demonstrate the sensor's repeatable performance and high voiding efficiency. Our integrated bladder system can be used for real-time bladder volume monitoring at various stages of voiding and actuator operation. Furthermore, it ensures a low level of urinary retention owing to the high voiding efficiency of the actuator. This soft system demonstrated on a bladder may serve as a model for augmenting other organs as well.

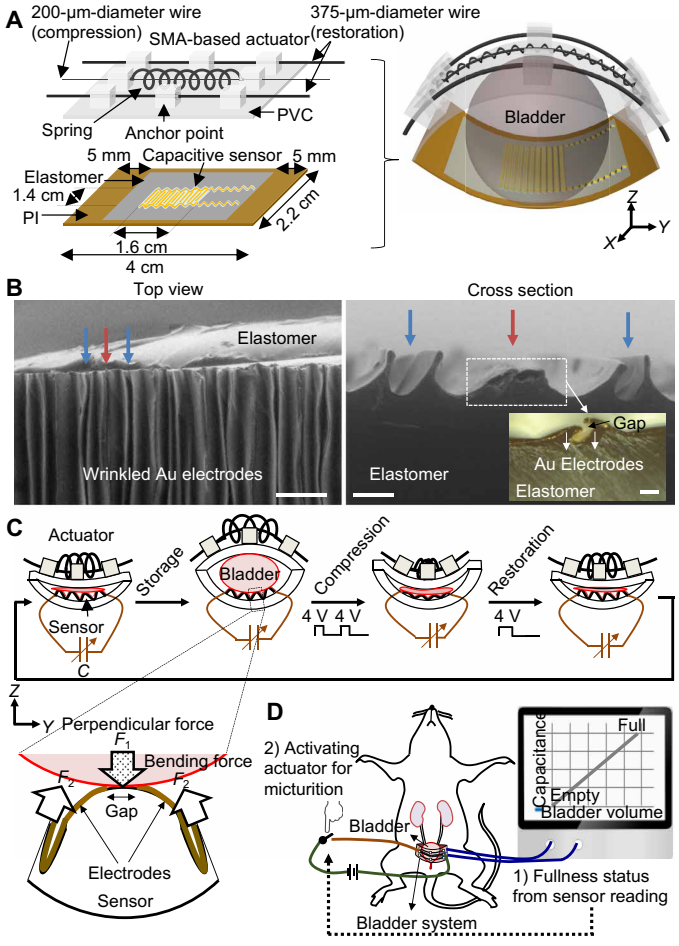

Fig. 1. The sensing-actuation bladder system and micturition. (**A**) The schematic of the integrated capacitive sensor with the SMA-based actuator. (**B**) The top view SEM (scale bar, 500 μm), magnified cross-section SEM (scale bar, 100 μm), and (Inset) the optical image of the wrinkled interdigitated electrodes (scale bar, 50 μm). The blue arrows present the formed two wrinkles on each adjacent electrode, and the orange arrow shows the gap between the electrodes. (**C**) The schematic side view of the integrated bladder system during the storage, compression, and restoration phases. The enlarged schematic side view presents two adjacent electrodes with a gap, perpendicular (F_1), and bending (F_2) forces applied to the sensor during the storage phase. (**D**) The schematic of the micturition stages by using the integrated bladder system for a rat.

RESULTS

Bladder voiding sensing actuation system

The integrated bladder voiding system, illustrated in Fig. 1A, consists of a flexible SMA-based actuator and a capacitive interdigitated sensor. The sensor's 125-μm-thick polyimide (PI) substrate was connected by using 70-μm-thick Kapton tape for the width of both side edges to the actuator's180-μm-thick polyvinyl chloride (PVC) substrate. The PVC substrate upper face contains the SMA components, while the sensor was positioned on the inner face of the PI substrate. The bladder was placed between the two substrates covering the sensor as shown in Fig. 1A. The system sensor and actuator components are explained below.

Bladder-inspired wrinkled interdigitated capacitive sensor

Pelvic nerve afferents monitor bladder fullness during the storage phase (*36*). The afferent fibers in the bladder muscle consist of two groups of strain and volume receptors (*36*, *37*). The bladder wall volume and strain receptors can be activated by perpendicular force and strain, respectively (*36*, *37*). In our design, we attempted to mimic the bladder sensory receptors with a polymeric capacitive sensor, designed in such a way that it responds to both perpendicular and bending force changes. The sensor consists of a polymeric layer with wrinkled interdigitated electrodes. The top view scanning electron microscopy (SEM) image of the wrinkles is shown in Fig. 1B.

The interdigitated electrodes were fabricated separately and then laminated on a 1-mm-thick double-sided adhesive acrylic elastomer layer that was prestretched up to 200%. The acrylic elastomer layer was then released and adhered to the PI substrate. The cross-sectional SEM image of the sensor is also presented in Fig. 1B. The release of the acrylic elastomer layer caused the formation of two wrinkles on each electrode and one wrinkle between two electrodes with a 50-μm gap as shown in Fig. 1B, which also presents the optical image of the electrodes gap. The fabrication steps for the interdigitated sensor are explained in Materials and Methods and are illustrated in fig. S1.

The side-view schematics in Fig. 1C (storage) present the system operation during the storage phase. The sensor capacitance change during bladder filling is used as bladder volume indicator. The sensor softness allows the sensor tension change due to bending. Furthermore, the wrinkles improve the sensitivity of the sensor to the perpendicular force applied by the bladder filling. The enlarged schematic in Fig. 1C illustrates the perpendicular (F_1) and bending (F_2) forces that can be exerted on the sensor during storage. The procedure for preparing a wrinkled sensor and its characteristics under individually applied F_1 and F_2 forces are explained later.

SMA-based actuator

Actuator's SMA components consist of a nitinol (NiTi) spring, a 200-μm-diameter NiTi wire for the compression phase, and two 375-μm-diameter NiTi wires for the restoration phase (Fig. 1A). The 200-μm-diameter SMA wire was passed through the SMA spring, while the spring and the two 375-μm-diameter NiTi wires were attached to the three-dimensional (3D)–printed anchor points on the PVC substrate. Silicone tubing was used for thermal insulation of the 375-μm-diameter SMA wires. Copper tape was used to connect the two 375-μm-diameter SMA wires. By applying a voltage to the 200-μm-diameter wire, its temperature increases, causing the spring temperature reaches the 45°C transition temperature. The spring starts to shrink due to heating, forcing the PVC substrate to bend and compress the bladder (Fig. 1C, compression). The PVC substrate transparency allows the bladder observance during the actuator activation. Following the compression phase, a voltage is applied to the 375-μm-diameter SMA wires to straighten the spring, flattening the PVC substrate for the restoration phase (Fig. 1C, restoration), thereby relaxing the spring and PVC substrate pressure on the bladder. The bladder can then fill normally until the next activation. The temperature characteristics and repeatable SMA-based actuator performance during compression and restoration phases were previously investigated (*34*). The SMA-based actuator integration with the TENG sensor in (*34*) caused a substantial voiding efficiency reduction from 80 to 43% due to thick and multilayered sensor structure. The soft wrinkled capacitive sensor in this work is not only capable of detecting bladder volume but also has minimal interference with the SMA-based actuator's voiding efficiency. The schematic illustration in Fig. 1D presents the system-assisted micturition for a rat. Once the bladder volume reaches the full state based on the sensor reading, the user can initiate voiding by activating the actuator.

The sensitivity of wrinkled sensor to perpendicular and bending forces

The setup used for introducing wrinkles to electrodes is illustrated in Fig. 2A. The acrylic elastomer layer was affixed to a linear stage. The elastomer layer was then prestretched up to 200%. Then, the patterned interdigitated electrodes in fig. S1 (vi) were laminated on

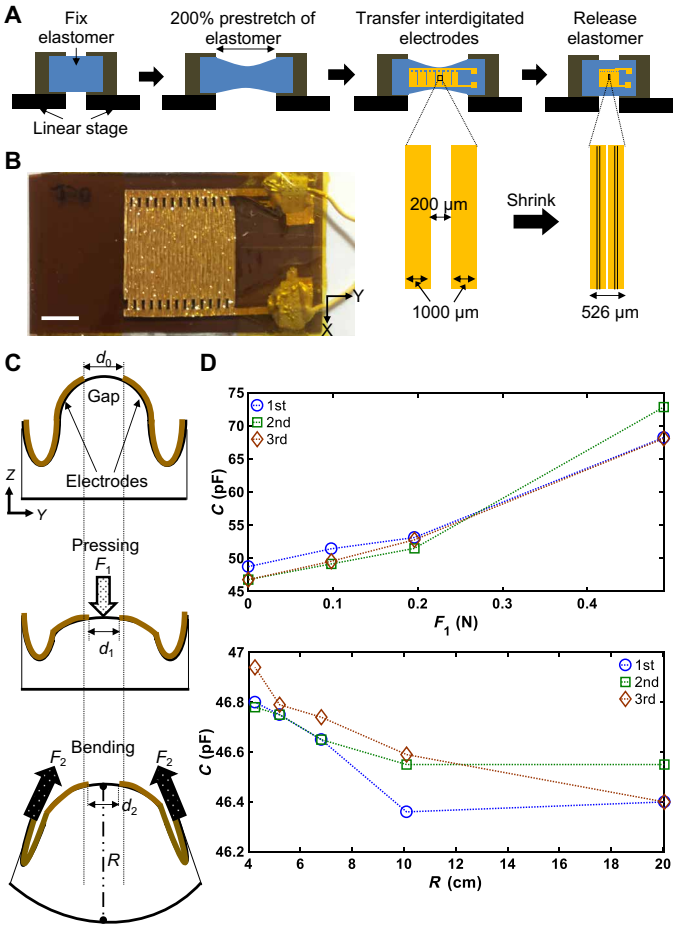

Fig. 2. The interdigitated capacitive sensor and multifunctional sensing. (**A**) The steps for preparing wrinkled interdigitated electrodes on a prestretched acrylic elastomer. (**B**) The optical top view image of the wrinkled electrodes. Scale bar, 5 mm. Photo credit: Faezeh Arab Hassani, National University of Singapore and University of Tokyo. (**C**) Schematic view of the gap without deformation and with deformation due to the perpendicular force (F_1) and bending forces (F_2). (**D**) The capacitance characteristics of the sensor due to changes of F_1 and bending radius (R).

the prestretched acrylic elastomer layer and was then released from the linear stage. The width of two adjacent electrode fingers with a gap of 200 μm was reduced from 2200 to 526 μm after the acrylic elastomer layer relaxation (Fig. 2A). The optical image of the sensor is shown in Fig. 2B. The gap deformation effect on the capacitance during force application was investigated. Figure 2C shows the schematic cross section of two electrode fingers with a gap (d_0) before and after deformation due to pressure and bending. A series of weights were placed on the sensor to investigate the capacitance changes due to pressure and perpendicular forces. The capacitance change versus force characteristics are shown in Fig. 2D. The experiment was repeated for three iterations. The capacitance increased from ~45 to ~70 pF by increasing the force from 0 to 0.5 N due to gap reduction between the two electrodes (d_1). The PI substrate was then bent within a 4 to 20 cm bending radius (R) range to investigate its bending sensitivity (Fig. 2D). The bending experiment was also repeated for three iterations. The bending radius reduction and, consequently, the gap (d_2) resulted in capacitance increase from ~46 to

~47 pF. The sensor gauge factor measurement is discussed in the Supplementary Materials and is illustrated in fig. S2. During the bladder filling phase, the sensor experienced an increase of both perpendicular and bending forces thanks to its wrinkled structure. We found that by placing the sensor on the outer face of the PI substrate, the capacitance reduction from bending canceled the increased capacitance from the perpendicular force. As a result, it is important to place the sensor on the PI substrate inner face for sensor sensitivity improvement.

In vitro characterization of the sensing-actuation system

The in vitro setup in Fig. 3A was used to characterize the integrated system during the storage, compression, and restoration phases. A rubber balloon with a size similar to a rat's bladder (i.e., 1-cm diameter) was placed between the two flexible system substrates. A syringe pump was used to fill the balloon with various filling rates of 100, 300, and 500 µl/min since the bladder may have various filling rates depending on daily liquid intake. An LCR [Inductance (L), capacitance (C), and resistance (R)] meter (BR5812, MCP Lab Electronics) was used to measure the capacitance change at a 1-kHz measurement frequency during each experimental phase. The water voided from the balloon was measured with a microbalance during the actuator activation and balloon voiding.

The balloon was filled up to 1 ml during the storage phase. Figure 3B shows the sensor capacitance change versus balloon volume for filling rates of 100, 300, and 500 µl/min. The cross-sectional images in Fig. 3B present the integrated system and balloon status before and after filling. An average capacitance increase of about 1 pF was observed for the three filling rates. For all three storage experiments, the balloon started to overflow at about 0.8 ml; therefore, the capacitance curve slope was reduced for volumes larger than 0.8 ml. The filling rate (500 µl/min) showed a slightly higher capacitance change of about 1.1 pF with a sensitivity of about 1.4 nF/liter. The sensitivity is defined by $\Delta C/V_b$, where, $\Delta C = C - C_0$ is the capacitance change, C is the capacitance value at each time (t), and C_0 is the original capacitance value. The capacitance change independence to the filling rate in Fig. 3B resembles the bladder wall volume receptors that only respond to the bladder volume changes irrespective of the filling rate (*36*, *37*). The sensor capacitance increase was due to both the sensor bending and the pressure applied from the balloon. ΔC characteristics of the interdigitated sensor in Fig. 3B is compared to a parallel plate capacitive sensor, which was only half as sensitive as the interdigitated capacitive sensor, in fig. S3. The details of the parallel plate sensor fabrication process appear in the Supplementary Materials.

After reaching the maximum balloon capacity without water overfilling (V_b), the compression phase was initiated by applying voltage to the 200-µm-diameter SMA wire and heating the spring around it, causing its length reduction due to shape memory effect. This forced balloon voiding due to downward PVC substrate bending. After applying two voltage pulses of 4 V to the 200-µm-diameter SMA wire, the balloon maximum voiding percentage was achieved. The ON state duration was 20 s to ensure achieving the maximum spring contraction, while the OFF state duration was kept at 40 s, long enough to cool the spring down and allow some of its elongated length recovery. Figure 3C presents the integrated bladder system voiding percentage and capacitance characteristics during two voltage pulses. The balloon started to void after the voltage was turned ON, and voiding continued even after turning the voltage OFF at t = 20 s. However, the voiding rate began to slow down from t = 20 s onward. A voiding percentage of about 65% was achieved before commencing

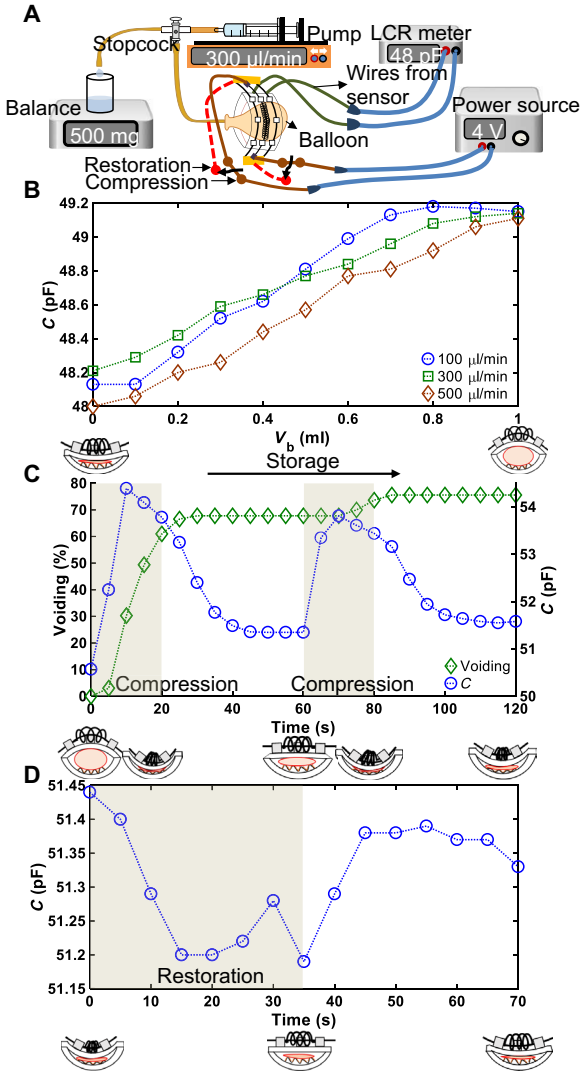

Fig. 3. In vitro characteristics of the integrated bladder system. (**A**) The schematic of the in vitro setup. (**B**) The capacitance characteristics of the sensor during the storage phase with three filling rates. (Inset) Schematic side views of the system before and after the storage phase completion. (**C**) The voiding (diamond dotted line) and capacitance (circle dotted line) characteristics of the integrated bladder system during the compression phase. (Inset) Schematic side views of the system during various compression phase points. The gray sections present the duration of turning the voltage ON. (**D**) The capacitance characteristics of the integrated bladder system during the restoration phase. (Inset) Schematic side views of the system during various points of the restoration phase. The gray section presents the duration of turning the voltage ON.

the second voltage pulse at t = 60 s. The balloon started to void at t = 65 s and the voiding percentage reached to about 75% after turning the voltage OFF at t = 80 s. The voiding percentage was almost constant from t = 80 s onward. The sensor capacitance showed a sudden rise within 10 s after initiating the first voltage pulse. Then, the capacitance gradually decreased until the voltage turned OFF. After the voltage was OFF, the capacitance reduced more abruptly during a 20-s period and became constant afterward. A similar trend was observed during the second voltage pulse. However, the peak capacitance value for the second voltage pulse is about 1 pF lower than that

of the first voltage pulse due to the balloon voiding and perpendicular force reduction from the balloon on the sensor. The integrated system cross-sectional views are presented in Fig. 3C at t = 0, 20, 60, 80, and 120 s. Table S1 summarizes the values of V_b, C_0, and voiding percentage for all of the integrated bladder system experiments. The system repeatability test during the storage and compression phases was performed, and capacitance characteristics are shown in fig. S4.

This was followed by applying a voltage of 4 V to the 375-μm-diameter SMA wires to elongate the spring length for separating the PVC substrate from the PI substrate. For the restoration phase, the ON state persisted up to 35 s to allow enough time for heating and straightening of the 375-μm-diameter SMA wires. Figure 3D presents the sensor capacitance characteristics during the restoration phase. Application of 4 V to the 375-μm-diameter SMA wires during the restoration phase caused straightening of the bent wires; the bending of PI substrate decreased, resulting in the capacitance reduction. Voltage removal at t = 35 s caused a bending increase, and the capacitance started to recover to its original value. The cross-sectional views of the integrated system and balloon are presented in Fig. 3D at t = 0, 35, and 70 s.

After the integrated system implantation inside the body, the actuator's operational information can be obtained from the integrated sensor. If the actuator activation does not result in micturition, it may be attributed to the actuator operation. However, if the appropriate actuator operation can be verified by the sensor, then the possibility of the urinary obstruction should be explored. For this reason, we activated the actuator in the presence of an obstructed outlet (incomplete voiding), closed stopcock (no voiding), and complete voiding to determine the capability of the sensor in predicting a possible urinary obstruction. The details on the experiment for both compression and restoration phases are described in the Supplementary Materials and are presented in fig. S4.

Electrode encapsulation is necessary to avoid possible body fluid interaction. Both a 600- and a 1200-nm-thick parylene encapsulation for the sensor were tried, but the 600-nm-thick parylene encapsulation was used in our experiments to circumvent an increase in the Young's modulus and the sensor layer rigidity. The sensor capacitance characteristics with 600- and 1200-nm-thick parylene encapsulation layers during the storage phase are compared in fig. S5. The capacitance characteristics of the 1200-nm-thick parylene sensor during three iterations of the compression and restoration phases are also described in the Supplementary Materials and are shown in fig. S5. The results are described in detail in the Supplementary Materials.

In vivo characterization of the integrated bladder system

The setup for in vivo testing of the integrated bladder system on an anesthetized rat's bladder is shown in Fig. 4A. The experiments were performed on two adult females (rats 1 and 2) and one adult male (rat 3). The surgical procedure details are presented in Materials and Methods. A syringe pump was used to fill the bladder with saline with a flow rate of 300 μl/min, similar to a rat's filling rate (*34*). The capacitance changes were monitored by an LCR meter, while the voided urine collected from the bladder was measured by a microbalance. Figure 4B shows the implanted integrated bladder system on the bladder of rat 1. The capacitance curve of the sensor during the storage phase is presented in Fig. 4C. Since the bladder started to leak after filling to about 0.7 ml, the capacitance change in Fig. 4C is only displayed for the maximum volume of 0.7 ml. The cross-sectional images in Fig. 4C present the status of the integrated bladder system and bladder before and after the storage phase completion. The capacitance value increased from about 48 pF in Fig. 3B to about 6.4 nF as soon as the sensor was placed in contact with bladder tissue and body fluids. This is mainly due to the body fluids ionic effect in contact with the sensor electrodes (*38*). An increase of about 0.5 nF in capacitance and a sensor sensitivity of 0.7 μF/liter was observed during the storage phase. The bladder filling during

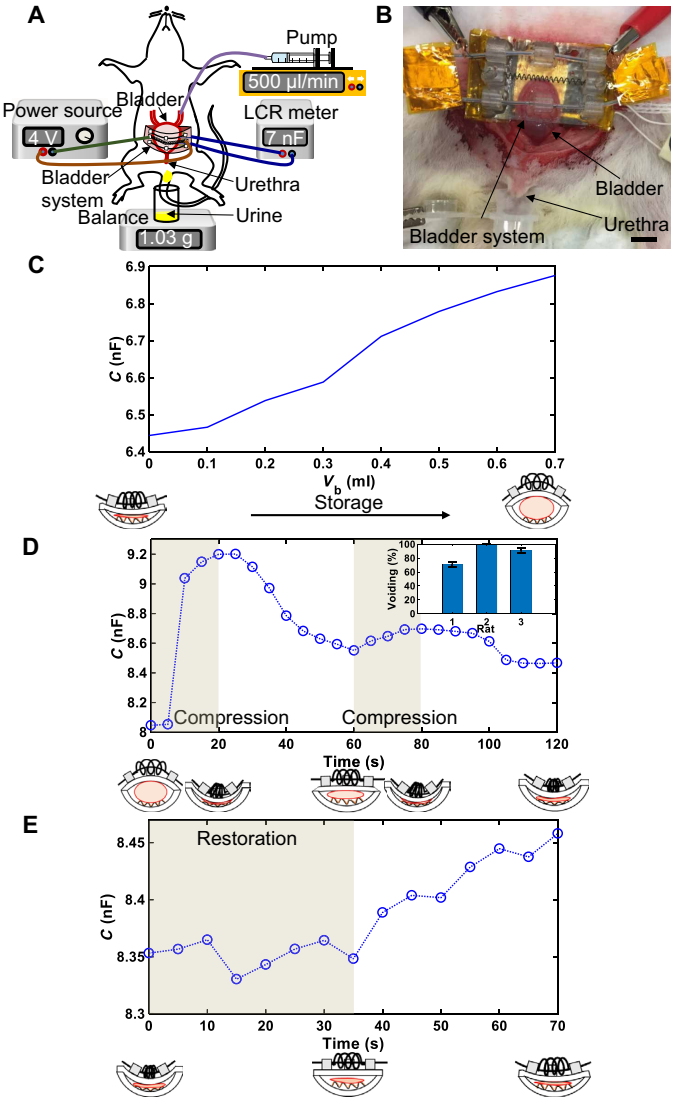

Fig. 4. In vivo characteristics of the integrated bladder system. (**A**) The schematic of the in vivo setup. (**B**) The implanted integrated bladder system on an anesthetized rat's bladder. Scale bar, 5 mm. Photo credit: Faezeh Arab Hassani, National University of Singapore and University of Tokyo. (**C**) The capacitance characteristics of the sensor during the bladder storage. (Inset) Schematic side views of the system before and after the storage phase completion. (**D**) The capacitance characteristics of the integrated bladder system during the compression phase. (Inset) The voiding percentage for the three rats. (Below inset) Schematic side views of the system before and after the compression phase completion. The gray sections present the duration of ON voltage. (**E**) The capacitance characteristics of the integrated bladder system during the restoration phase. (Inset) Schematic side views of the system before and after the restoration phase completion. The gray sections present the duration of ON voltage.

the storage phase and the capacitance changes monitored with the LCR meter are shown in movies S1 and S2, respectively.

As in the case of the in vitro experiment, two voltage pulses of 4 V were applied to the 200-μm-diameter SMA wire for the compression phase. The capacitance curve (Fig. 4D) shows a sudden capacitance increase after turning voltage ON at t = 5 s, and the capacitance started decreasing following voltage removal. A sensitivity of about 1.6 μF/liter was observed for the sensor during the first voltage application. A similar behavior was observed for the second pulse after turning the voltage ON. However, the peak capacitance value is about 0.4 nF smaller than that of the first pulse due to voiding of the bladder by 74.23%. The side-view images in Fig. 4D illustrate the status of the bladder and integrated bladder system at various compression phase points. The bladder status during the compression phase and capacitance changes are shown in movies S3 and S4, respectively. The storage phase for V_b of 0.7 ml and the compression phase for rats were repeated for three iterations, and the capacitance characteristics of the integrated bladder system are described in the Supplementary Materials and are presented in fig. S6. The voiding percentage for all rats is presented as an inset to Fig. 4D.

The capacitance curve of the integrated bladder system during the restoration phase is shown in Fig. 4E. As shown in Fig. 3D, the capacitance was reduced following the 4-V application to the 375-μm-diameter SMA wires. By turning the voltage OFF, the capacitance increased due to the reduction of the PI substrate bending. The cross-sectional views of the integrated bladder system and bladder are presented in Fig. 4E, at various restoration phase steps. Movies S5 and S6 present the bladder and integrated bladder system status and the capacitance changes during the restoration phase, respectively.

The capacitance characteristics of the integrated bladder system during both the compression and restoration phases for a complete voiding case, as well as the no voiding case, due to urethra obstruction for rat 1 are presented in fig. S6. The second peak was not observed for the no voiding and incomplete curves in fig. S6 compared to the no voiding and incomplete voiding curves for the balloon in fig. S4C. This difference is due to the larger Young's modulus of the rubber balloon in comparison with the bladder. Therefore, the balloon caused a larger normal force to be exerted on the sensor during actuator activation, resulting in a visible second peak even for the incomplete voiding cases. The details of the characteristics are provided in the Supplementary Materials. Movies S7 and S8 demonstrate the bladder and integrated bladder system status and the capacitance changes during the compression phase for the no voiding case, respectively. The parylene thickness effect on the implanted integrated bladder system performance in rat 3 is explained in the Supplementary Materials and is presented in fig. S7.

DISCUSSION

In the current work, we present an integrated bladder system. The necessity of integrating a soft and thin sensor for achieving repeatable sensing capabilities without limiting the required voiding efficiency has been emphasized. The integrated system presented in this work serves as a potential candidate for future on-time and efficient neurogenic bladder voiding. A soft and thin sensor enables continued measurement from the bladder even when fully distended. The bladder system actuator achieves a very high emptying level. As a result, the voiding efficiency, about 71 to 100%, is achieved successfully by the integrated bladder system.

First, owing to the capacitive sensor flexibility, the voiding efficiency was not affected by the sensor integration. Two consecutive voltage pulses were applied to the bladder. However, a large portion of voiding was achieved after the completion of first voltage pulse, especially for the bladder with properties softer than those of the balloon. In this case, application of the second voltage pulse is not required. If the voiding percentage is low, the actuator should be activated for a second voltage pulse to check the second capacitance peak value. If the second peak value is similar to the first peak, there is a possibility of urethra obstruction.

Second, the sensitivity of the sensor to both force and tension improved the capacitance changes during the storage phase. Therefore, this multifunctional sensor can provide a more accurate and repeatable bladder volume estimation. Increasing the encapsulation layer thickness can improve the long-term effect of body fluids on capacitance value drift; however, the sensor sensitivity will be degraded owing to a higher sensor stiffness. As a result, the thickness of the encapsulation layer should be considered as a key design parameter for the integrated bladder system, and a long-term validation on awake animal models is necessary for achieving this. Several consecutive actuator activations may cause the sensor deformation and capacitance value drift. However, the necessity to void the bladder four to five times every day gives enough time for the sensor to return to its original state before the next activation.

Next, we showed the implantation of the integrated bladder system for three different bladder sizes from V_b = 0.2 to 0.7 ml, showing the scalability of a single design for a range of bladder sizes. Especially if a patient's bladder size changes over time (*39*), the system should still show reasonable functionality. The sensor sensitivity, particularly for V_b smaller than 0.7 ml, can be improved by introducing more gaps to the structure. For future wireless device deployment on an awake animal model, an ultrasound is required for full bladder volume estimation and a precalibration test. Observing the sensor reading during an intentional and gradual bladder filling through urethra can be used for the precalibration. Moreover, multiple periodic calibrations may also be required, since the sensor capacitance value depends on the bladder muscle properties that may change over time. These calibrations will be used to find the correlation between capacitance changes and the volume for defining a notification alarm when the bladder volume reaches at least 70% and the consequent activation of the actuator.

In conclusion, the soft bladder system is a technology, which considers both sensing and actuation to act on similarly soft and stretchable body organs. The bladder system achieves a high voiding efficiency through the integrative operation. This design can serve as a model for other soft and distensible organs like blood vessels, heart, and the gastrointestinal system where both sensing and actuation are needed to achieve functions like pumping and peristalsis under soft actuation and control.

MATERIALS AND METHODS

Materials

SMA wires (200- and 375-μm diameter) have a transition temperature of 70°C (DYNALLOY Inc.). The NiTi spring (Kellog's Research Labs), with a transition temperature of 45°C, has an original length of 1 cm, but it was then stretched up to 2.4 cm and affixed to two 3D-printed anchor points (VeroClear-RGD810; Objet260 Connex3, Stratasys) by using ultraviolet (UV) curable glue. The outer body spring diameter

is 1.65 cm, with a 250-μm-diameter wire. The total number of spring turns is 21. The PI and thermoplastic polyurethane layer were purchased from UBE Industries Ltd. and NSK Echomark, respectively. Common PVC binding sheets were used as the SMA component substrate. A 70-μm-thick Kapton tape was purchased from element14. Copper tape was used to connect the two 375-μm-diameter SMA wires and for further connection of the SMA wires and capacitive sensor to the source power and the LCR meter. The UV curable glue was also used to attach the anchor points on the PVC substrate.

Interdigitated capacitive sensor fabrication

The fabrication steps are presented in fig. S1. (i) A 1-μm-thick polyethylene terephthalate (PET) substrate (DuPont Teijin Films) was laminated onto a Kapton film adhesive (Teraoka Seisakusho Co. Ltd.) layer for easier handling. (ii) A 100-nm-thick gold (Au) layer was thermally deposited on the PET/Kapton film adhesive layer following the predeposition of a 3-nm-thick chromium (Cr) adhesive layer. (iii) The Au/PET/Kapton film adhesive layer was adhered from the Au side to a glass stage that was slightly wetted with water. A green laser cutting machine (MD-T1010, KEYENCE) was used to pattern the interdigitated electrodes in the Au/PET/Kapton film adhesive layer with the electrodes finger's width of 1000 μm and a gap of 200 μm. (iv) Another Kapton film adhesive layer was laminated on the laser-patterned Au/PET/Kapton film adhesive layer to remove the pattern from the glass stage. Then, the gold surface was encapsulated with 600-nm-thick parylene (diX-SR, Daisan Kasei Co. Ltd.). (v) An adhesive layer (CM-0003-R1A, GRAPHTEC) was used to delaminate the patterned Au/PET layer from the Kapton film adhesive layers. (vi) The patterned Au/PET layer was then laminated onto the prestretched adhesive acrylic elastomer layer [Very high bond (VHB) tape, 3M] from the PET side. (vii) Since the acrylic elastomer layer adhesion was larger than the Kapton film adhesive layer, it could easily be separated from the Au/PET/elastomer layer. The prestretching force for the acrylic elastomer layer was then removed; thus, the Au/PET layer deformed to a wrinkled structure. The wrinkled Au/PET/acrylic elastomer layer was then attached to a 125-μm-thick PI substrate.

Surgical procedure

The experiments were performed on two adult females (300 g) and one adult male (500 g) Sprague-Dawley rats. The animal care and use procedures were approved by the Institutional Animal Care and Use Committee of the National University of Singapore. The procedure was carried out in accordance with the R18-0753 protocol. The animal was anaesthetized by 1.5% isofluorane through inhalation. For providing analgesic, buprenophrine (0.05 mg/kg) was used, and to prevent dehydration of the animal, normal saline (0.2 to 0.5 ml/10 g) was subcutaneously injected. After exposing the bladder through an abdominal incision, the integrated bladder system was affixed to the bladder and filled with normal saline through a cannula inserted into the left ureter to carry out the experiments.

SUPPLEMENTARY MATERIALS

Supplementary material for this article is available at http://advances.sciencemag.org/cgi/content/full/6/18/eaba0412/DC1

View/request a protocol for this paper from *Bio-protocol*.

REFERENCES AND NOTES

1. J. D. Bronzino, *The Biomedical Engineering Handbook* (CRC Press, Springer, 2000).
2. C. Choi, Y. Lee, K. W. Cho, J. H. Koo, D.-H. Kim, Wearable and implantable soft bioelectronics using two-dimensional materials. *Acc. Chem. Res.* **52**, 73–81 (2019).
3. S. Hannah, P. Brige, A. Ravichandran, M. Ramuz, Conformable, stretchable sensor to record bladder wall stretch. *ACS Omega*. **4**, 1907–1915 (2019).
4. T. Shahid, D. Gouwanda, S. G. Nurzaman, A. A. Gopalai, Moving toward soft robotics: A decade review of the design of hand exoskeletons. *Biomimetics* **3**, E17 (2018).
5. P. Polygerinos, N. Correll, S. A. Morin, B. Mosadegh, C. D. Onal, K. Petersen, M. Cianchetti, M. T. Tolley, R. F. Shepherd, Soft robotics: Review of fluid-driven intrinsically soft devices; manufacturing, sensing, control, and applications in human-robot interaction. *Adv. Eng. Mater.* **19**, 1700016 (2017).
6. S. Choi, H. Lee, R. Ghaffari, T. Hyeon, D.-H. Kim, Recent advances in flexible and stretchable bio-electronic devices integrated with nanomaterials. *Adv. Mater.* **28**, 4203–4218 (2016).
7. L. Xu, S. R. Gutbrod, Y. Ma, A. Petrossians, Y. Liu, R. C. Webb, J. A. Fan, Z. Yang, R. Xu, J. J. Whalen III, J. D. Weiland, Y. Huang, I. R. Efimov, J. A. Rogers, Materials and fractal designs for 3D multifunctional integumentary membranes with capabilities in cardiac electrotherapy. *Adv. Mater.* **27**, 1731–1737 (2015).
8. K. B. Justus, T. Hellebrekers, D. D. Lewis, A. Wood, C. Ingham, C. Majidi, P. R. LeDuc, C. Tan, A biosensing soft robot: Autonomous parsing of chemical signals through integrated organic and inorganic interfaces. *Sci. Robot.* **4**, eaax0765 (2019).
9. H. A. Sonar, A. P. Gerratt, S. P. Lacour, J. Paik, Closed-loop haptic feedback control using a self-sensing soft pneumatic actuator skin. *Soft Robot.* **7**, 22–29 (2019).
10. H. Watanabe, Y. Azuma, Periodical measurement of urine volume in the bladder during sleep: Temporary volume reduction suggestive of absorption. *Int. J. Urol.* **23**, 182–187 (2016).
11. K. I. Tudor, R. Sakakibara, J. N. Panicker, Neurogenic lower urinary tract dysfunction: Evaluation and management. *J. Neurol.* **263**, 2555–2564 (2016).
12. M. Przydacz, P. Denys, J. Corcos, What do we know about neurogenic bladder prevalence and management in developing countries and emerging regions of the world? *Ann. Phys. Rehabil. Med.* **60**, 341–346 (2017).
13. W. Al Taweel, R. Seyam, Neurogenic bladder in spinal cord injury patients. *Res. Rep. Urol.* **7**, 85–99 (2015).
14. A. D. Asimakopoulos, C. De Nunzio, E. Kocjancic, A. Tubaro, P. F. Rosier, E. Finazzi-Agrò, Measurement of post-void residual urine. *Neurourol.Urodyn.* **35**, 55–57 (2016).
15. J. C. Misra, S. Maiti, Peristaltic pumping of blood through small vessels of varying cross-section. *J. Appl. Mech. Trans. ASME.* **79**, 061003 (2010).
16. S. Dirven, F. Chen, W. Xu, J. E. Bronlund, J. Allen, L. K. Cheng, Design and characterization of a peristaltic actuator inspired by esophageal swallowing. *IEEE/ASME Trans. Mechatronics.* **19**, 1234–1242 (2014).
17. T. Someya, Z. Bao, G. G. Malliaras, The rise of plastic bioelectronics. *Nature* **540**, 379–385 (2016).
18. A. Miyamoto, S. Lee, N. F. Cooray, S. Lee, M. Mori, N. Matsuhisa, H. Jin, L. Yoda, T. Yokota, A. Itoh, M. Sekino, H. Kawasaki, T. Ebihara, M. Amagai, T. Someya, Inflammation-free, gas-permeable, lightweight, stretchable on-skin electronics with nanomeshes. *Nat. Nanotechnol.* **12**, 907–913 (2017).
19. J. Rivnay, H. Wang, L. Fenno, K. Deisseroth, G. G. Malliaras, Next-generation probes, particles, and proteins for neural interfacing. *Sci. Adv.* **3**, e1601649 (2017).
20. H. Shim, K. Sim, F. Ershad, P. Yang, A. Thukral, Z. Rao, H.-J. Kim, Y. Liu, X. Wang, G. Gu, L. Gao, X. Wang, Y. Chai, C. Yu, Stretchable elastic synaptic transistors for neurologically integrated soft engineering systems. *Sci. Adv.* **5**, eaax4961 (2019).
21. K. Sim, Z. Rao, Z. Zou, F. Ershad, J. Lei, A. Thukral, J. Chen, Q.-A. Huang, J. Xiao, C. Yu, Metal oxide semiconductor nanomembrane–based soft unnoticeable multifunctional electronics for wearable human-machine interfaces. *Sci. Adv.* **5**, eaav9653 (2019).
22. D. Yan, T. M. Bruns, Y. Wu, L. L. Zimmerman, C. Stephan, A. P. Cameron, E. Yoon, J. P. Seymour, Ultracompliant carbon nanotube direct bladder device. *Adv. Healthc. Mater.* **8**, e1900477 (2019).
23. A. D. Mickle, S. M. Won, K. N. Noh, J. Yoon, K. W. Meacham, Y. Xue, L. A. McIlvried, B. A. Copits, V. K. Samineni, K. E. Crawford, D. H. Kim, P. Srivastava, B. H. Kim, S. Min, Y. Shiuan, Y. Yun, M. A. Payne, J. Zhang, H. Jang, Y. Li, H. H. Lai, Y. Huang, S. Il Park, R. W. Gereau, J. A. Rogers, A wireless closed-loop system for optogenetic peripheral neuromodulation. *Nature* **565**, 361–365 (2019).
24. F. Stauffer, Q. Zhang, K. Tybrandt, B. Llerena Zambrano, J. Hengsteler, A. Stoll, C. Trüeb, M. Hagander, J.-M. Sujata, F. Hoffmann, J. Schuurmans Stekhoven, J. Quack, H. Zilly, J. Goedejohann, M. P. Schneider, T. M. Kessler, W. R. Taylor, R. Küng, J. Vörös, Soft electronic strain sensor with chipless wireless readout: Toward real-time monitoring of bladder volume. *Adv. Mater. Technol.* **3**, 1800031 (2018).
25. X. Yang, C. An, S. Liu, T. Cheng, V. Bunpetch, Y. Liu, S. Dong, S. Li, X. Zou, T. Li, H. Ouyang, Z. Wu, W. Yang, Soft artificial bladder detrusor. *Adv. Healthc. Mater.* **7**, e1701014 (2018).
26. M. N. Dakurah, C. Koo, W. Choi, Y.-H. Joung, Implantable bladder sensors: A methodological review. *Int. Neurourol. J.* **19**, 133–141 (2015).

27. M. K. Kim, H. Kim, Y. S. Jung, K. M. A. Adem, S. S. Bawazir, C. Stefanini, H. J. Lee, Implantable bladder volume sensor based on resistor ladder network composed of conductive hydrogel composite. *Conf. Proc. IEEE Eng. Med. Biol. Soc.* **2017**, 1732–1735 (2017).
28. S. Lee, W. Y. X. Peh, J. Wang, F. Yang, J. S. Ho, N. V. Thakor, S.-C. Yen, C. Lee, Toward bioelectronic medicine—Neuromodulation of small peripheral nerves using flexible neural clip. *Adv. Sci.* **4**, 1700149 (2017).
29. J. Wang, Z. Xiang, G. G. L. Gammad, N. V. Thakor, S.-C. Yen, C. Lee, Development of flexible multi-channel muscle interfaces with advanced sensing function. *Sens. Actuators A Phys.* **249**, 269–275 (2016).
30. E. T. Roche, M. A. Horvath, I. Wamala, A. Alazmani, S.-E. Song, W. Whyte, Z. Machaidze, C. J. Payne, J. C. Weaver, G. Fishbein, J. Kuebler, N. V. Vasilyev, D. J. Mooney, F. A. Pigula, C. J. Walsh, Soft robotic sleeve supports heart function. *Sci. Transl. Med.* **9**, eaaf3925 (2017).
31. E. Fattorini, T. Brusa, C. Gingert, S. E. Hieber, V. Leung, B. Osmani, M. D. Dominietto, P. Büchler, F. Hetzer, B. Müller, Artificial muscle devices: Innovations and prospects for fecal incontinence treatment. *Ann. Biomed. Eng.* **44**, 1355–1369 (2016).
32. Y. Dang, M. Stommel, L. K. Cheng, W. Xu, A soft ring-shaped actuator for radial contracting deformation: Design and modeling. *Soft Robot.* **6**, 444–454 (2019).
33. F. A. Hassani, G. G. L. Gammad, R. P. Mogan, T. K. Ng, T. L. C. Kuo, L. G. Ng, P. Luu, N. V. Thakor, S.-C. Yen, C. Lee, Design and anchorage dependence of shape memory alloy actuators on enhanced voiding of a bladder. *Adv. Mater. Technol.* **3**, 1700184 (2017).
34. F. A. Hassani, R. P. Mogan, G. G. L. Gammad, H. Wang, S.-C. Yen, N. V. Thakor, C. Lee, Toward self-control systems for neurogenic underactive bladder: A triboelectric nanogenerator sensor integrated with a bistable micro-actuator. *ACS Nano* **12**, 3487–3501 (2018).
35. D.-H. Kim, R. Ghaffari, N. Lu, S. Wang, S. P. Lee, H. Keum, R. D'Angelo, L. Klinker, Y. Su, C. Lu, Y.-S. Kim, A. Ameen, Y. Li, Y. Zhang, B. de Graff, Y.-Y. Hsu, Z. Liu, J. Ruskin, L. Xu, C. Lu, F. G. Omenetto, Y. Huang, M. Mansour, M. J. Slepian, J. A. Rogers, Electronic sensor and actuator webs for large-area complex geometry cardiac mapping and therapy. *Proc. Natl. Acad. Sci. U.S.A.* **109**, 19910–19915 (2012).
36. V. P. Zagorodnyuk, M. Costa, S. J. H. Brookes, Major classes of sensory neurons to the urinary bladder. *Auton. Neurosci.* **126–127**, 390–397 (2006).
37. A. Kanai, K.-E. Andersson, Bladder afferent signaling: Recent findings. *J. Urol.* **183**, 1288–1295 (2010).
38. J. S. Chae, N.-S. Heo, C. H. Kwak, W.-S. Cho, G. H. Seol, W.-S. Yoon, H.-K. Kim, D. J. Fray, A. T. E. Vilian, Y.-K. Han, Y. S. Huh, K. C. Roh, A biocompatible implant electrode capable of operating in body fluids for energy storage devices. *Nano Energy* **34**, 86–92 (2017).
39. A. E. Finkbeiner, The aging bladder. *Int. Urogynecol. J.* **4**, 168–174 (1993).
40. A. D. Valentine, T. A. Busbee, J. W. Boley, J. R. Raney, A. Chortos, A. Kotikian, J. D. Berrigan, M. F. Durstock, J. A. Lewis, Hybrid 3D printing of soft electronics. *Adv. Mater.* **29**, 1703817 (2017).
41. R. Nur, N. Matsuhisa, Z. Jiang, M. O. G. Nayeem, T. Yokota, T. Someya, A highly sensitive capacitive-type strain sensor using wrinkled ultrathin gold films. *Nano Lett.* **18**, 5610–5617 (2018).
42. D. R. Hickling, T.-T. Sun, X.-R. Wu, Anatomy and physiology of the urinary tract: Relation to host defense and microbial infection. *Microbiol. Spectr.* **3**, 10.1128/microbiolspec. UTI-0016-2012, (2015).

Acknowledgments

Funding: F.A.H. is an International Research Fellow of Japan Society for the Promotion of Science [Invitational Fellowships for Research in Japan (Long-term)]. The authors would like to acknowledge financial support from the following research grant: NRF-CRP10-2012-01 "Peripheral Nerve Prostheses: A Paradigm Shift in Restoring Dexterous Limb Function" from the National Research Foundation (NRF), Singapore. **Author contributions:** F.A.H., H.J., T.Y., T.S., and N.V.T. designed research. F.A.H. fabricated the actuator and integrated bladder system and conducted the system characterization and in vivo implantation. H.J. fabricated and characterized the sensor. F.A.H., H.J., T.Y., T.S., and N.V.T. analyzed data. F.A.H. and H.J. wrote the paper. F.A.H., H.J., T.Y., T.S., and N.V.T. read the paper. **Competing interests:** The authors declare that they have no competing interests. **Data and materials availability:** All data needed to evaluate the conclusions in the paper are present in the paper and/or the Supplementary Materials. Additional data related to this paper may be requested from the authors.

Submitted 6 November 2019
Accepted 10 February 2020
Published 1 May 2020
10.1126/sciadv.aba0412

Citation: F. Arab Hassani, H. Jin, T. Yokota, T. Someya, N. V. Thakor, Soft sensors for a sensing-actuation system with high bladder voiding efficiency. *Sci. Adv.* **6**, eaba0412 (2020).

Soft sensors for a sensing-actuation system with high bladder voiding efficiency

F. Arab Hassani, H. Jin, T. Yokota, T. Someya and N. V. Thakor

Sci Adv **6** (18), eaba0412.
DOI: 10.1126/sciadv.aba0412